Hindawi
Wireless Communications and Mobile Computing
Volume 2022, Article ID 7344498, 15 pages
https://doi.org/10.1155/2022/7344498

Research Article

Research on Terrain Sensing Method and Model Prediction for Height Adjustment of Sugarcane Harvester Base Cutter

Liang Zhao, Shengjie Jiao, Chao Wang, and Jun Zhang

Highway Maintenance Equipment National Engineering Laboratory, Chang'an University, Xi'an 710064, China

Correspondence should be addressed to Jun Zhang; zhangjun@chd.edu.cn

Received 7 May 2022; Revised 28 May 2022; Accepted 4 June 2022; Published 18 June 2022

Academic Editor: Chia-Huei Wu

The sugarcane plantations in China occupy large areas of undulated terrain. During the operation of a sugarcane harvester, the operator's vision is severely obstructed, and the height of the cutter needs to be adjusted frequently, resulting in low sugarcane harvesting efficiency and difficulty in ensuring harvesting quality. However, the current diversified non-contact methods are unable to distinguish or penetrate the interference well to provide feedback regarding the change in terrain height. Based on the proposed contact sensing method, a contact terrain sensing device is designed for application to the sugarcane harvester, and the orthogonal test is carried out with the standard orthogonal table $L_9(3^4)$ to study the influence of the working parameters of the device on the terrain height sensing performance. Through the analysis of the working principle of the device, three factors (moving speed, rotational torque, and preload) are tested in three levels, and index systems of the Fréchet distance and residual standard deviation are proposed. The range and variance analysis methods are used to statistically analyze the test results to determine the primary and secondary orders of operation parameters. Then, the regression model was obtained by regression analysis on the influencing factors. After analysis, the influences of moving speed and rotating torque were found to be the most significant, and the influence of preload was the smallest. The results show that the average relative errors between the experimental values and predicted model values of the Fréchet distance and residual standard deviation were 3.46% and 2.48%. According to the practical applications of the sugarcane harvester and the data of the two indexes, the optimal value ranges of moving speed (km/h) and rotating torque (Nm) are determined as (1.57, 1.75) and (0.73, 0.86), respectively, which provide a certain reference for the subsequent application of the terrain sensing device to sugarcane harvesters.

1. Introduction

Sugarcane is the main economic crop of southern China. As a perennial plant, it is planted once every three years on average and is an important raw material for the production of sugar and bioethanol. Owing to increasing labor costs, mechanized harvesting of sugarcane has become a development trend [1]. Guangxi is the main sugarcane-producing area in China. The hilly landforms and complex field conditions in this area make mechanized harvesting of sugarcane more challenging. In particular, if the sugarcane cutting point is too low, it will damage the foundation of the sugarcane and reduce the germination rate of the sugarcane in the following year; in contrast, if the cutting point is too high, it will not only cause a significant loss in sugarcane harvesting but also increase the risk of root breakage [2]. Therefore, an appropriate cutting height has become one of the key drivers for improving the efficiency of mechanized sugarcane harvesting [3]. A fast and accurate perception of sugarcane terrain fluctuations is the key to self-adaptive adjustment of the cutter height. It also improves the quality of mechanized sugarcane cutting and meets the needs of future precision agricultural harvesting. However, because the terrain of sugarcane planting area is very uneven and fluctuating, it is difficult to achieve only manual operation when feedback on terrain height changes are not provided. As shown in Figure 1, the operator's line of sight is covered by

Figure 1: Sugarcane harvester work site (FFP: first-person perspective).

disturbances such as sugarcane stems, leaf crowns, and weeds, making it difficult to accurately locate the ground and greatly aggravating the difficulty of cutting sugarcane.

Scholars at home and abroad have conducted research on terrain sensors in the field of agriculture, which can be divided into non-contact and contact. The non-contact sensing method can avoid physical contact between soil and sugarcane and has higher accuracy and cost. It primarily uses digital image recognition (contour extraction), 3D fusion point clouds, ultrasonic sensors, laser sensors, and video technology [4–10]. However, existing non-contact technology is mostly suitable for crops with significant background differences and obvious features that are easy to identify, and the sugarcane harvesting environment is affected by factors such as weeds, sugarcane stems and leaves, dust, and droppers, which makes the application of this method quite challenging. Contact-sensing methods are relatively traditional. In the early days, Podmore and Huggins proposed a linear profile meter to measure the sand topography, using a linear variable differential transformer (LVDT) as a feedback sensor [11]; the roller chain topography measurement have also been proposed to be simple and efficient [12, 13]. Thomesn et al. pointed out that the application of the static contact measurement method above is limited [14] and is not applied to real-time measurement feedback. In the field of agricultural machinery, Xie et al. used the rotation of the "feeler" to feedback the change of the ground and then converted it into the cutting height as a signal generator for the height control of the header of the combine harvester [15]. Suomi and Oksanen used the average value of the towed wheel and the distance measurement of multiple ultrasonic sensors to obtain the ground profile change to achieve automatic depth control of the planter [16]. Xie et al. installed an angular displacement sensor and an inclination sensor. The plowing depth is measured by the suspension unit of the tractor, and the standard deviation of the topographic measurement data was 8.19 mm [17]. Xia et al. used an angle sensor to measure the surface flatness to control the tillage depth of the tractor and verified that automatic adjustment is better than mechanical adjustment [18]. It can be seen that the contact terrain perception method can be better adapted to the complex and changeable farmland.

However, most current research on adjusting actuators for terrain profile changes focus on signal processing or parameter optimization of the control system, and few in-depth studies on the effect of terrain signal acquisition have been conducted. Dynamic contact sensing is complex. There are many soil parameters in sugarcane fields, and the input excitation of the soil topography is generally a random signal. The accuracy and scientificity of the numerical simulation results cannot be confirmed; in particular, the contact relationship between the sensing device and soil is difficult to determine, which usually involves too many assumptions, and the theoretical formula is not universally applicable. Even according to the analysis of field conditions of sugarcane fields, when studying the performance of the terrain sensing device on a sugarcane field, it is difficult to select the best optimization parameters. Therefore, based on the proposed contact sensing method, we designed a terrain sensor suitable for sugarcane harvesters and used an orthogonal test method to study the influence of the working parameters of the terrain sensor on the performance of terrain height sensing.

The main contributions of this study are as follows:

(1) A contact terrain sensing method and device were proposed and designed. The encoder was used to feed back the rotation angle of the sensing towed board (STB), and a mathematical model for sensing the rotation angle of the STB and the terrain height was established

(2) A test bench and soil model of the terrain sensor were built, and nine sets of experiments with different working parameters were designed using the orthogonal test table $L_9(3^4)$

(3) The Fréchet distance (FD) and residual standard deviated (RSD) were proposed to describe the curve similarity and illustrate the curve fit, respectively, and as the test index, the range and variance were used to analyze the data, and the influence order and trend of the test factors were determined

(4) A nonlinear regression analysis prediction mathematical model was established. The performance of the sensor was verified via error analysis on the experimental data and model data, and the quantitative relationship between the influencing factors and the experimental indicators was determined

The remainder of this paper is organized as follows. Section 2 introduces the design of the test device and the factor analysis and the orthogonal test in detail. Section 3 expounds the test process and results of the influencing factors of the terrain sensing device. Section 4 develops the range and variance analysis, establishes the regression model, and discusses its limitations. Finally, Section 5 provides a summary.

2. Materials and Methods

2.1. Experimental Setup. To adapt to the complex cane field terrain, the design block diagram of the terrain sensing test bench is shown in Figure 2, including a driving device, terrain height sensor, infrared distance sensor, and terrain signal processing

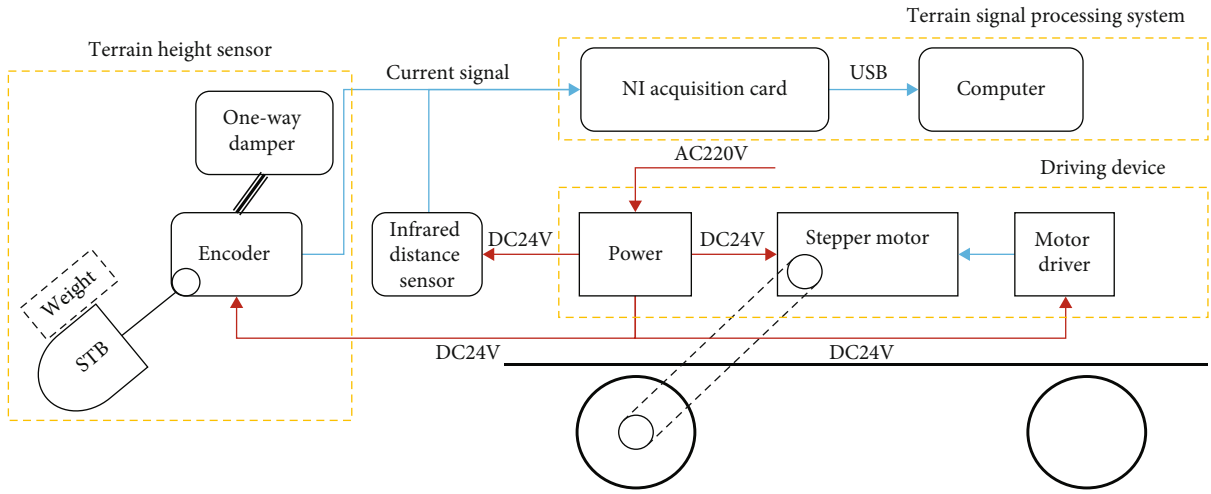

Figure 2: Design block diagram of terrain induction test bench.

system. The power of the driving device was provided by a stepping motor to realize the movement of the test bench on the soil groove track; the terrain height sensor was composed of an STB (rubber), encoder, and a one-way damper. The encoder is an important component in terrain signal acquisition. The absolute value encoder of POSITAL was used to collect the rotation angle of the towed board in real time. The 4-20 mA current signal was input to the national instruments (NI) acquisition card, and its resolution was 12 bits (resolution 0.08°). The terrain height expectation curve was realized via the infrared distance sensor produced by SICK, with a resolution of 0.1 mm and a repeatability of ≥0.5 mm. The terrain signal processing system consisted of an NI 9223 board and a LabVIEW graphical programming software, and the sampling frequency was set to 1 kHz [17]. Figure 3 shows the terrain sensing test bench built according to the design.

In fact, in China, a large number of related researchers and manufacturers have attempted to use different contact methods to realize the sensing of sugarcane terrains. It is worth mentioning that through on-the-spot investigations in sugarcane fields, the STB used in this study was designed with a small curvature in the middle, and the bottom was in contact with the ground with a semicircle. After many experiments and analyses, the installation direction, shown in Figure 2, was more conducive to feed back the terrain profile, which can minimize the phenomenon of early response when encountering sudden changes in terrain.

Terrain height was calculated using the rotation angle of the STB. Using the uphill stage as an example, an absolute coordinate system was established. The negative direction of the x-axis was the moving direction of the STB, and the positive direction of the z-axis was the height of the terrain. A geometric model of the terrain height and angle of the STB was established, as shown in Figure 4. Point A is the initial contact point between the STB and the soil slope, and point B is the final contact point between the STB and the soil slope. The relationship between the STB angle and terrain height can be expressed as

$$\begin{cases} h = l\cos\theta + r\cos\mu, \\ h' = l\cos\theta' + r\cos\mu', \\ \Delta h = h - h' = l\left(\cos\theta - \cos\theta'\right) + r\left(\cos\mu - \cos\mu'\right), \end{cases} \tag{1}$$

where l is the distance from the center point of the rotating shaft to the center point of the bottom arc; r is the radius of the bottom arc; l and r are fixed values; h and h' are the vertical heights from the contact points A and B to the center point of the rotating shaft, respectively; θ and θ' are the angles between the l and the x-axis at points A and B, respectively; μ is the angle between r and the z-axis at point A; μ' is the angle between r and the z-axis at point B; and Δh is the height difference (that is, the terrain height value) of the contact point in the z-axis direction after sensing the movement of the STB. Since $r << l$, to simplify the experiment, we ignore r, and l is directly expressed as the distance from the center point of the rotating shaft to the contact point.

2.2. Experimental Material. The topography of the sugarcane planting areas in China varies greatly; most of the sugarcane planting areas are in hilly areas, and most of the slopes are between 5° and 25°. In addition, sugarcane fields have been washed by rain for a long time, which makes the topography of sugarcane fields more complex and changeable. Therefore, we built a 1 : 1 soil (cinnamon soil) model in the soil tank test bench of the Chang'an University laboratory and used tools such as a spirit level and a tape measure to calibrate the size. Models ①, ②, and ③ include slope terrain and step terrain, in which slopes S_1 and S_2 in model ① are 10°, and slopes S_3 and S_4 in model ② are 30°. The detailed dimensions of the model are shown in Figure 5. Model ① was used to simulate common sugarcane planting slopes, model ② was used to represent local extreme slopes, and model ③ was used to represent abrupt terrain.

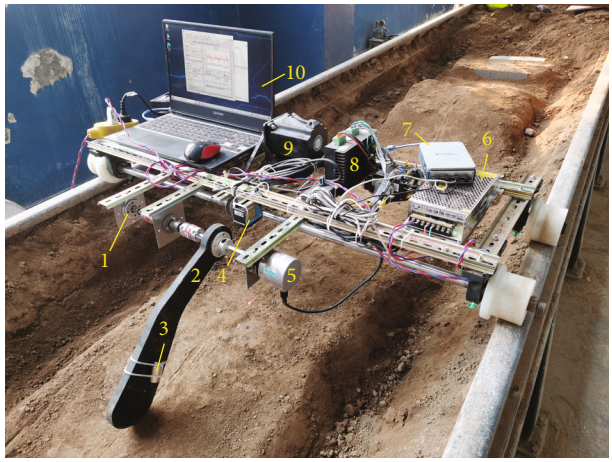

Figure 3: Terrain sensing test bench. (1) One-way damper. (2) STB. (3) Weight. (4) Infrared distance sensor. (5) Encoder. (6) Power. (7) NI acquisition card. (8) Motor driver. (9) Stepper motor. (10) Computer.

In the test, bolts were used to fasten the terrain sensing device to the rear side of the drive device bracket. The drive device was placed horizontally between the rails of the soil tank bench. With the movement of the driving device, the STB can maintain good surface contact with the soil model in the vertical and horizontal directions and can freely rotate following the ups and downs of the soil model.

2.3. Design of Experiments. According to the dynamic theory, when a rigid body rotates around a fixed axis, the product of the angular acceleration of its motion and the moment of inertia is equal to the sum of the moments of all external forces on the rigid body on the axis. Thus, the second-order linear differential equation of the STB can then be expressed as

$$J\frac{d^2\theta}{dt^2} = -C\frac{d\theta}{dt} - \frac{1}{2}mgl\cos\theta, \tag{2}$$

where J is the moment of inertia of the STB. C denotes the damping coefficient of the damper. m is the mass of STB. Combined with the terrain sensing device, it can be observed that the moving speed, rotating torque, and mass of the STB of the terrain sensing device all impact the accuracy of terrain sensing. Based on this, orthogonal experiments were conducted with them as influencing factors to determine the optimal working parameters of the designed terrain sensor.

According to Equation (2), the working parameters of the terrain height sensing device, namely, the moving speed, rotating torque, and preload (mass of STB), are considered the main factors. An orthogonal test was used to determine the primary and secondary orders of the parameters [19]. The orthogonal test method is a design method for arranging multifactor and multilevel combined experiments with the help of orthogonal tables using mathematical statistics and orthogonal principles [20]. A small number of typical combination experiments were used to achieve the purpose of comprehensive experiments; subsequently, the optimal combination in the experiments was determined from the analysis results. We analyzed the selection of the level according to the main influencing factors.

2.3.1. Determine the Level of Each Factor. Viator et al. evaluated sugarcane yield and quality in Brazil at 4.0, 4.8, and 5.6 km/h, respectively, and the results indicated that a forward speed of 4.0 km/h was ideal [21]. Martins et al. experimented with harvesting speeds of 3.0, 5.0, and 7.0 km/h, respectively, and concluded that the damage to the ratoon is more serious with an increasing moving speed [22], but the economic benefit of a moving speed of 7.0 km/h is the best [23]. Brazil is a large sugarcane-producing country, with flat terrain and large-scale planting areas. The overall efficiency of large-scale mechanized harvesting is relatively high [24]. However, owing to the large differences between China's sugarcane field environment and geographical features and those of Brazil and other planting areas, Chen et al. aimed to break the head rate and matched the best walking speed (1.0, 2.0, and 3.0 km/h) and cutter head speed of the sugarcane harvester [25]. In addition, according to our onsite inspection, the harvesting speed of local sugarcane harvester operators in Guangxi was maintained within the range of 1-1.8 km/h.

The rotating torque can provide a reverse damping torque to the STB to achieve the effect of damping vibration. The preload ensures that the STB is always close to the ground and avoids rebound after hitting the bottom after an instantaneous sudden change in the terrain. However, the mass of the towed board should not be too large; otherwise, scraping or deformation of the towed board will occur. The mass of the rubber-made towed board was 650 g. After many installation tests, the damper torques were 1 Nm and 2 Nm. The mass of the pallet was realized by adding weights at its center of mass, increasing by 300 g and 600 g, respectively.

According to the experimental conditions of three factors and three levels, a total of 27 comprehensive tests are required. The nine representative cross test points marked were selected through the orthogonal table $L_9(3^4)$, and each group of trials was repeated three times, as shown in Table 1. It should be noted that the interactions between the factors were not considered. Finally, according to the range analysis and variance analysis of the indicators, the influence degree, significance, and optimal combination of each factor on the indicators were studied.

2.3.2. Determine the Test Index

(1) Fréchet Distance. To compare and analyze terrain contour curves through the STB and infrared distance (ID) and measure the similarity of curves of different factor combinations, the Euclidean distance and dynamic time warping methods are usually employed. These are widely used in the field of time series data search, such as epidemics prevention and control analysis [26], traffic flow prediction [27], and speech recognition [28], etc. Without considering the limitations of data sample size, sampling frequency, and time series length, and only judging the similarity from the shape, we introduce a geometry-based FD algorithm [29, 30], which does not require a large number of training samples and has the

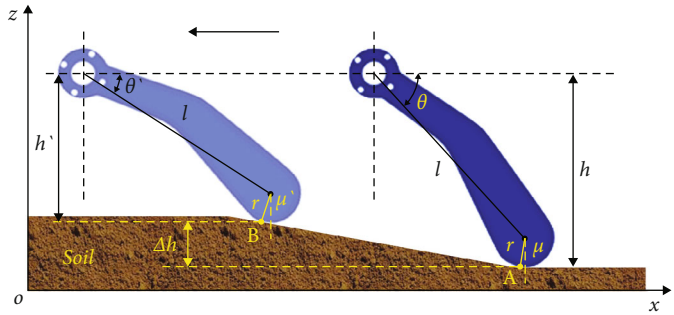

Figure 4: Relationship between the STB angle and terrain height.

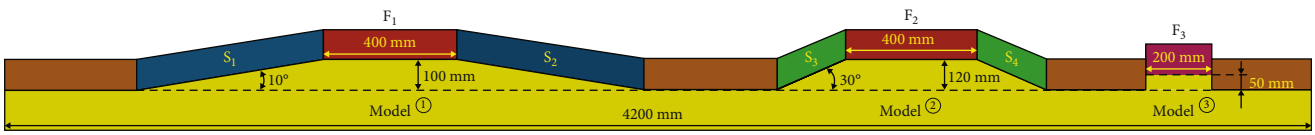

(a) Soil model

(b) Soil model building (with tracks)

Figure 5: Soil model test platform.

Table 1: Orthogonal test factor levels.

Factors	Units	Level 1	Level 2	Level 3
Moving speed	km/h	1	1.5	2
Rotating torque	Nm	0	1	2
Preload	g	0	300	600

advantages of being more intuitive and efficient. The FD algorithm is inspired by the human-dog distance model, which is used to find the longest dog leash that minimizes the distance between humans and dogs. The FD of the drag board perception curve Q and infrared ranging curve P are calculated according to the similarity function, as shown in Figure 6.

If $\alpha(t)$ and $\beta(t)$ represent the trajectory lengths of curves P and Q at time t, respectively, then they are also continuous incremental functions. Let $t \longrightarrow [0, 1]$, $\alpha(t) \longrightarrow [0, 1]$, $\beta(t) \longrightarrow [0, 1]$. Since the curves P and Q are known, the specific positions $P(\alpha(t))$ and $Q(\beta(t))$ of the curves P and Q can be determined by the length of the trajectory. The distance between $P(\alpha(t))$ and $Q(\beta(t))$ changes with the change in $\alpha(t)$ and $\beta(t)$, and the FD $F(P, Q)$ can be expressed as [31]

$$\delta F(P, Q) = \inf_{\alpha,\beta} \max_{t\in[0,1]} \{d(P(\alpha(t)), Q(\beta(t)))\}, \tag{3}$$

where $d(*,*)$ is the metric function (Euclidean distance) of curves P and Q, and inf is the infimum of the function value. The discrete FD is an approximation of the continuous FD that is typically used to approximate a given curve. The FD, discretized from the limit angle, can be expressed as

$$F(P, Q) = \lim_{\substack{n\longrightarrow\infty \\ \max_{k\in\{0,\cdots,n\}}\{|t_k - t_{k+1}|\}\longrightarrow 0}} \left\{ \inf_{\alpha,\beta} \left\{ \max_{t\in\{t_k\}_{k=0}^{n+1}} \{d(P(\alpha(t)), Q(\beta(t)))\} \right\} \right\}. \tag{4}$$

As t traverses all continuous values in the unit interval [0, 1], considering the structure of the internal nodes of the curve, the similarity between the two curves can be described more accurately.

(2) Residual Standard Deviation. Generally, in mathematical statistics, the deviation between the actual observed value and the estimated value of the sample model represents the residual, which is used to judge the convergence and to check whether there are errors or large cumulative errors in the process of regression smoothing. The standard deviation is used to measure the dispersion of data within the group. Most researchers usually use the standard deviation or the coefficient of variation to describe the data and do not consider the relationship with the speed. However, the fluctuation of the moving speed in our experimental factors is likely to have different degrees of influence on the standard deviation and the average value. Therefore, we calculated the vertical distance between the actual value and the expected value of each data point of the perception curve,

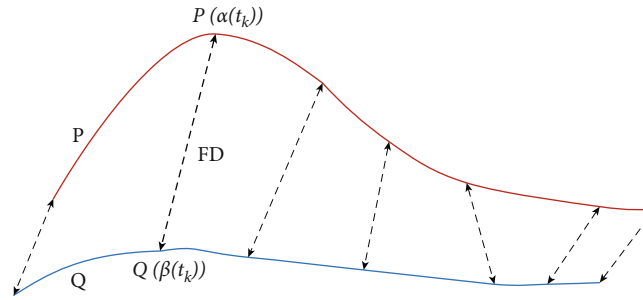

Figure 6: Fréchet distance measurement.

which is similar to the residual calculation, and the standard deviation of this distance was used as a variability indicator, which is the RSD [32]. RSD, which describes the variability of the data deviation from the fitted curve within a certain moving speed in this study, was used as the second result index in the orthogonal experiment. The smaller the RSD, the closer the predicted value of the model is to the actual experimental value and the better the fit of the experimental data in this group.

3. Results

Based on the $L_9(3^4)$ orthogonal table, the test plan was conducted nine times, and the measurement curve of the terrain height profile is shown in Figure 7. In order to keep the total length of the soil model at 4000 mm, we cut off the large deviation data of start and stop of the test bench. In Figure 7, the red line represents the ID curve. It can be observed from the figure that the red lines of each group of data are basically the same. It can also be observed that the height difference between the ID curve and the soil model (black dotted line) is caused by artificial errors during the model-building process. Simultaneously, the overall raw data oscillation is small, which also indicates that the terrain height measurement is reliable and can be used for the expected curve in this study. The blue line is the STB curve, and the contact point between the towed board and soil in the terrain sensing device lags behind the measurement point of the infrared distance sensor. We placed an iron sheet at the starting point of the soil model as the initial reference of the curve and moved the blue line to the x-axis direction to ensure that the red line and blue lines had the same initial point; the strong oscillations in the blue line data are partly due to the vibrations generated by the translation coupled with the system resonance, in particular, the oscillations generated by the uneven soil surface profile. The data were low-pass filtered using the LabVIEW software, and the cutoff frequency was set to 30 Hz to eliminate the influence of random errors and reflect the changing characteristics of the perception curve.

After processing the data using the MATLAB numerical simulation software, Table 2 summarizes the orthogonal array and experimental results of the FD and RSD of the nine trials, and the blank column (error column) was maintained. The calculated FD ranged from 27.35 mm (Test 7) to

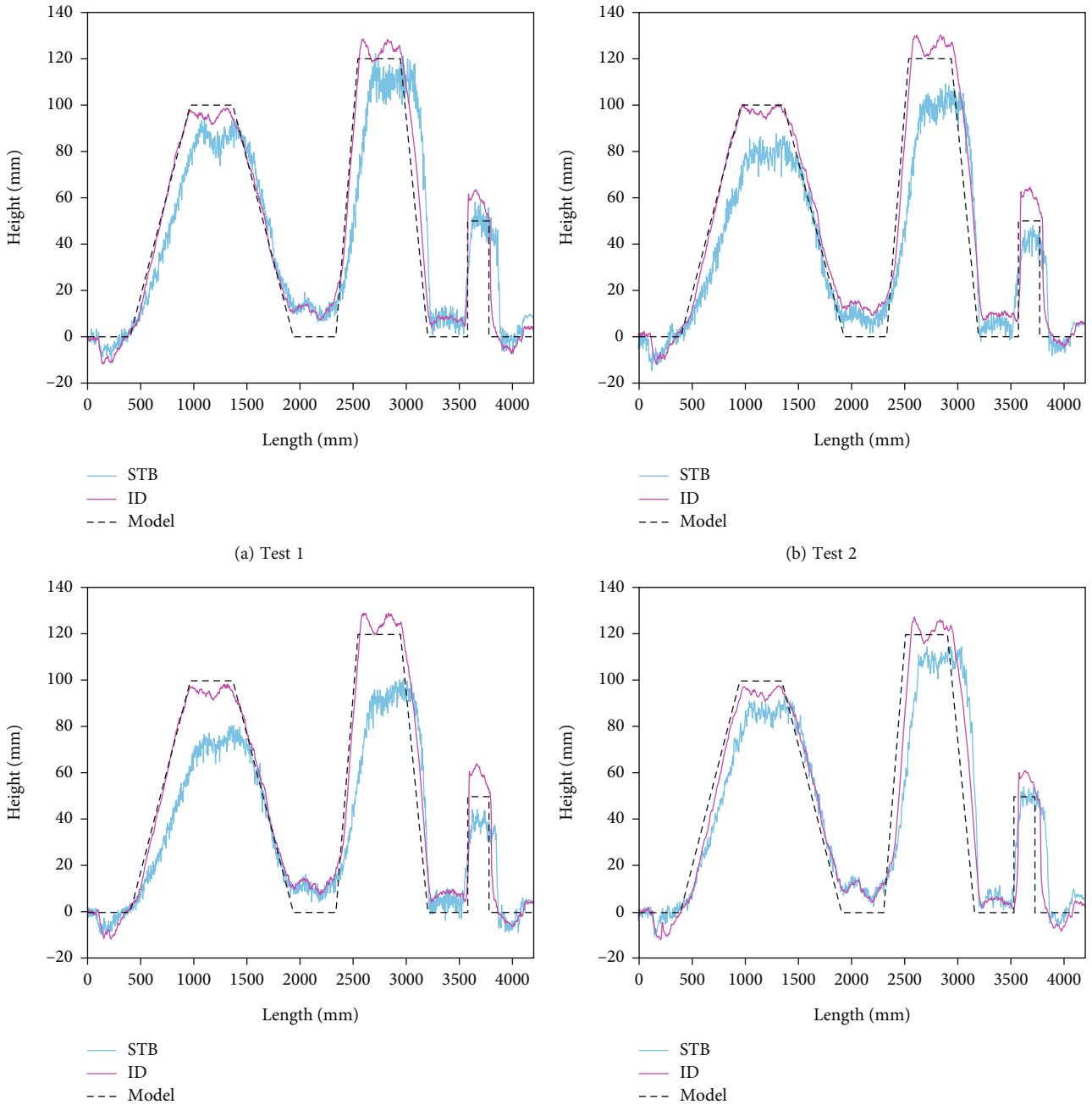

(a) Test 1

(b) Test 2

(c) Test 3

(d) Test 4

Figure 7: Continued.

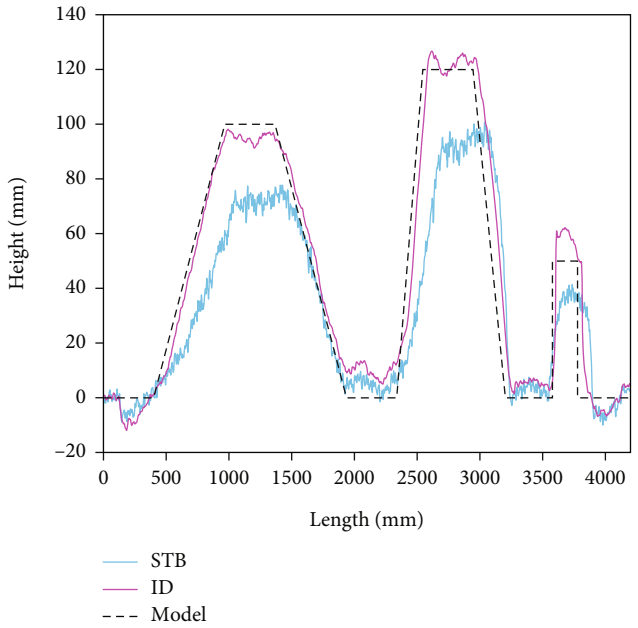

(e) Test 5

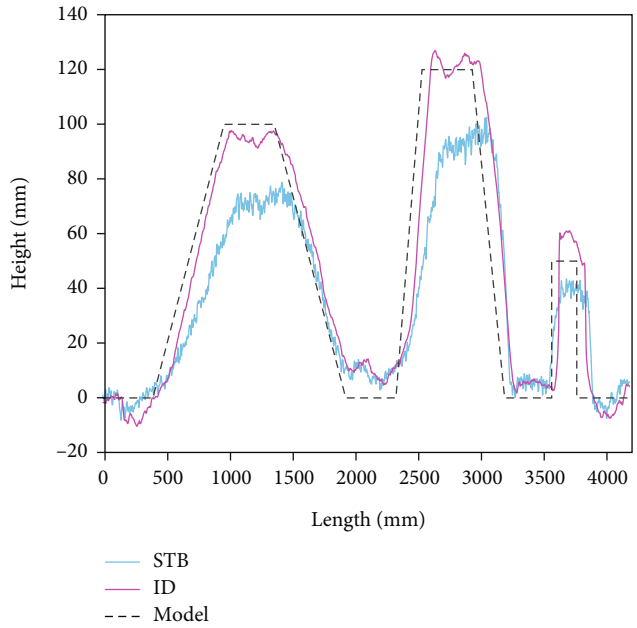

(f) Test 6

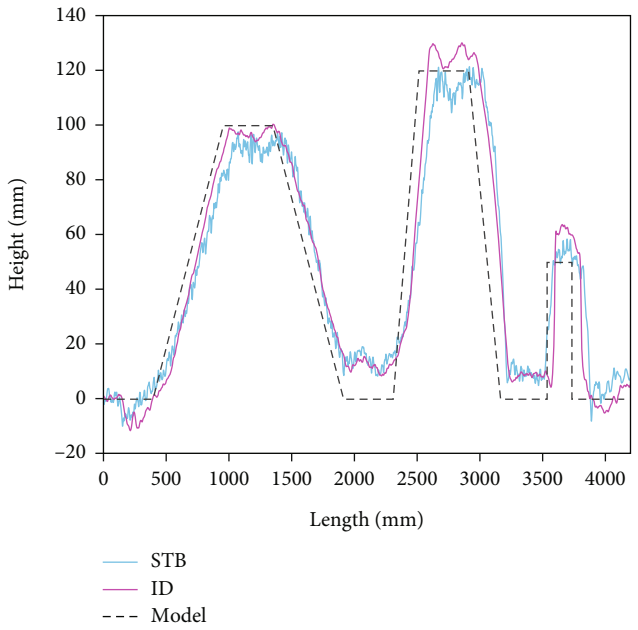

(g) Test 7

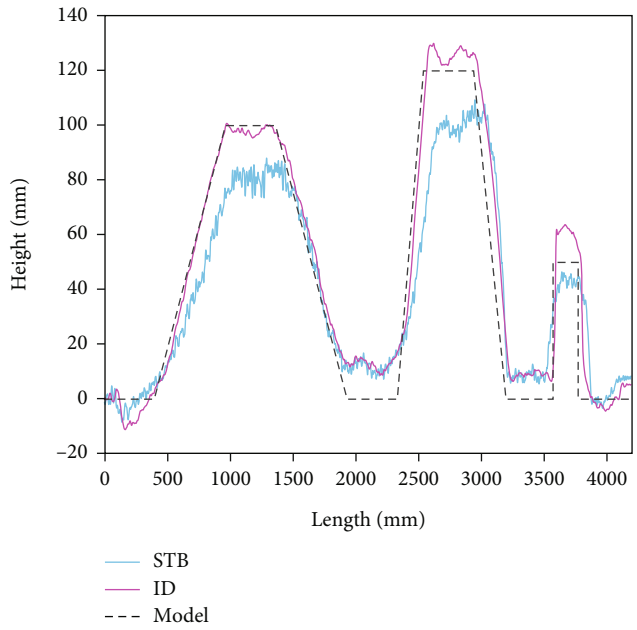

(h) Test 8

Figure 7: Continued.

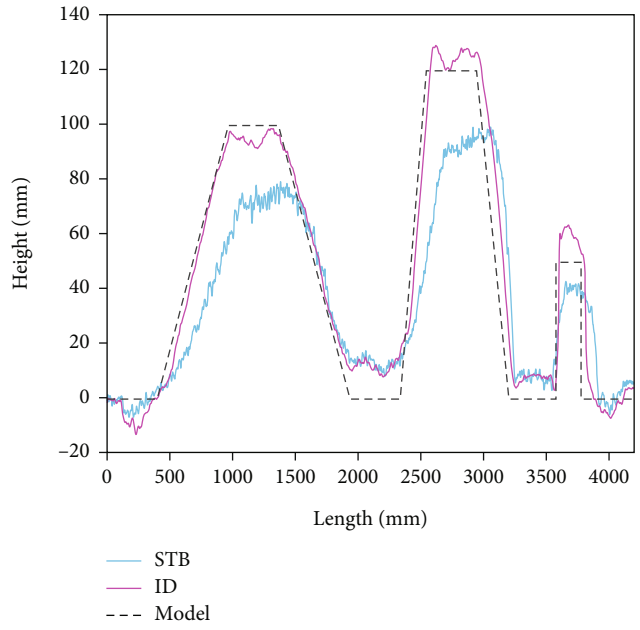

(i) Test 9

Figure 7: Measurement curve of terrain height profile.

Table 2: Orthogonal array and experimental results.

Test no.	Factors				Indexes	
	Moving speed (A) (km/h)	Rotating torque (B) (Nm)	Preload (C) (g)		FD (mm)	RSD (mm)
1	1 (1)	1 (0)	1 (0)	1	43.82	2.729
2	1	2 (1)	2 (300)	2	55.95	2.692
3	1	3 (2)	3 (600)	3	57.68	2.382
4	2 (1.5)	1	2	3	38.07	2.499
5	2	2	3	1	53.75	2.131
6	2	3	1	2	52.52	1.849
7	3 (2)	1	3	2	27.35	2.280
8	3	2	1	3	37.88	2.174
9	3	3	2	1	47.93	1.907

55.95 mm (Test 2), and the RSD ranged from 1.907 mm (Test 9) to 2.729 mm (Test 1).

According to the intuitive analysis in Figure 7 and Table 2, in the horizontal section of a terrain height of 0 mm, the blue line and the red line can basically maintain the overlap, and the intuitive reflection effect is good. The height difference between the two curves basically occurs in S_1 and S_3 (upper slope section), and F_1, F_2, and F_3 (top horizontal section) of models ①, ②, and ③, respectively, and the FD will basically occur at the intersection and inflection points of S_3 and F_2.

4. Statistical Analysis and Discussion

The purpose of the curve data analysis is to observe the influence trend of the experimental factors on the experimental result indicators, and whether there is a significant influence on the FD and RSD. In the orthogonal test, the range analysis method and the variance analysis method are usually used for analysis, which can be used to intuitively obtain the degree of influence of factors on the test data. The factor index analysis can obtain the analysis diagram to determine the optimal combination, and the analysis of variance can compare the error of the test to increase the accuracy of the test.

4.1. Range Analysis. The range analysis method uses mathematical statistics to calculate the range $\Re_j$ value of each column in the orthogonal test table. According to Equation (5), the optimal level combination and the primary and secondary orders of the influencing factors can be calculated. The greater the range, the greater the influence of this factor, which is the main factor. On the contrary, it is the secondary factor. At the same time, the smaller the index data, it indicates that the level of the corresponding index is the best.

Table 3: Range analysis of orthogonal test results.

Indexes	Level	Factors			
		A	B	C	
FD	K_1	157.45	109.24	134.22	145.50
	K_2	144.34	147.58	141.95	135.82
	K_3	113.16	158.13	138.78	133.63
	k_1	52.483	36.413	44.740	48.500
	k_2	48.113	49.193	47.317	45.273
	k_3	37.720	52.710	46.260	44.543
	$\mathfrak{R}$	44.29	48.89	7.73	11.87
RSD	K_1	7.803	7.508	6.752	6.767
	K_2	6.479	6.997	7.098	6.821
	K_3	6.361	6.138	6.793	7.055
	k_1	2.601	2.503	2.251	2.256
	k_2	2.160	2.332	2.366	2.274
	k_3	2.120	2.046	2.264	2.352
	$\mathfrak{R}$	1.442	1.37	0.346	0.288

$$\begin{cases} \mathfrak{R}_j = \max\left[K_{ij}\right] - \min\left[K_{ij}\right], \\ k_{ij} = \dfrac{K_{ij}}{s}, \end{cases} \tag{5}$$

where $\mathfrak{R}_j$ is the range of column j, K_{ij} is the sum of the test indexes at the level of factor i in column j, k_{ij} is the average of the sum of the test indexes at the level of factor i in column j, and s is the occurrence time of factor i in column j.

The test results in Table 2 are introduced into Equation (5), and the range analysis results are shown in Table 3. The influence of the three factors on FD is $R_B\,(48.89) > R_A\,(44.29) > R_C(7.73)$, and the effect of the three factors on the RSD is $R_A\,(1.442) > R_B\,(1.37) > R_C\,(0.346)$, indicating that the importance of the moving speed and rotating torque in the two indicators is different, while the preload presents a secondary factor, and its influence is the least significant. To analyze the influence of various factors on the test indicators more intuitively, the trend is shown in Figure 8.

With the k_{ij} data in Table 3, Figure 8 shows the effect of moving speed, rotating torque, and preload on FD and RSD. From Figure 8(a), it can be seen that the FD curves increases significantly with the doubling of the moving speed; however, the increase in the rotating torque significantly reduces the similarity, and the effect of the increase in the preload is not very obvious. It can be seen that the fast moving speed (2 km/h) and the loading of no rotating torque are beneficial for improving the similarity of the two curves, that is, improving the sensing effect of the STB. According to the analysis of the FD test results, the observed phenomenon was reasonable. This is because when the moving speed is doubled and increased, the data sampling points are also greatly reduced, which causes the rubber material towed board to filter out most of the unnecessary small terrain contours. However, according to a dynamic analysis of Equation (1), the increase in the moving speed leads to the acceleration of the floating angular speed of the STB. According to the characteristics of a one-way damper, this increases the rotation resistance of the encoder, which reduces the sensing effect of the terrain contour.

As shown in Figure 8(b), when the moving speed and rotating torque are doubled, the RSD of the STB curve decreases significantly. When the moving speed is 1.5–2 km/h, the impact on the index is slightly lower, the rotating torque decreases linearly, and the preload has no impact. It can be seen that the reduction in sampling points has a certain effect on reducing the fluctuation of the curve, and the influence trend of the increase in the rotating torque on the fluctuation of the curve is obvious, which is reduced by 0.439 mm. This analysis result is the opposite of that of the FD index. After analysis, it is considered that the STB rotation resistance filters part of the feedback to the terrain contour to a significant extent, and the volatility of the curve is reduced to a certain extent.

4.2. Variance Analysis. As a method of analyzing test data, variance analysis can be used to study whether the influence of factors on test results is significant; the setting of the relevant level of this factor can be controlled according to the significant results. The sum of squared deviations, degrees of freedom, and F value of each factor were calculated using formula (6), and the calculation results are shown in Table 4.

The variance analysis formula of orthogonal test is as follows:

$$\begin{cases} \mathrm{SS}_j = \dfrac{r}{n}\displaystyle\sum_{i=1}^{r} K_{ij}{}^2 - \dfrac{1}{n}\left(\sum_{k=1}^{n} y_k\right),^2 \\ df_j = r - 1, \\ F_j = \dfrac{\mathrm{MS}_j}{\mathrm{MS}_e} = \dfrac{\mathrm{SS}_j/df_j}{\mathrm{SS}_e/df_e}, \end{cases} \tag{6}$$

where n is the total number of tests, m is the number of test factors, r is the number of factor levels, SS_j is the sum of the squares of deviations of various factors ($j = 1, 2, \cdots, m$, and e), and y_k is the test result ($k = 1, 2, \cdots, n$).

F value for a given inspection level α, with $F_\alpha(df_j, df_e)$ checking the F distribution table. In this study, the given test level has $F_{0.05}(2, 4) = 6.94$, $F_{0.05}(2, 2) = 19$, $F_{0.01}(2, 4) = 18$, and $F_{0.01}(2, 2) = 99$. Usually, if $F_j > F_{0.05}\,(df_j, df_e)$, it shows that factor j has a significant impact on the test results; otherwise, it has no significant impact. According to Table 4, it can be seen that the factors that have the greatest impact on the FD are moving speed (A) and rotating torque (B), while $\mathrm{MS}_c < \mathrm{MS}_e$, indicating that the preload (C) has little impact on the test results. Therefore, it is included in the total error. The factors that have the greatest impact on RSD are moving speed (A) and rotating torque (B). Although the preload does not reach a significant level, the sum of squared deviations is larger than the sum of the squared deviations of the errors. This can be considered a secondary factor affecting the RSD in the latter stages.

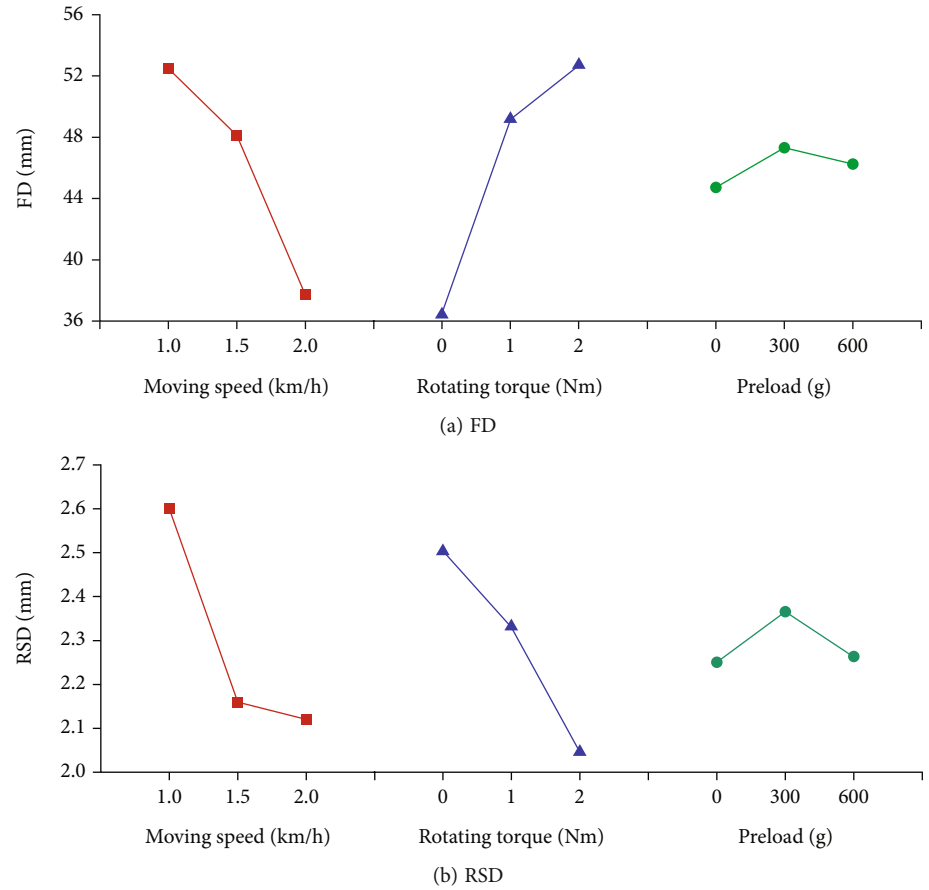

Figure 8: Influence of various factors on test indexes.

Table 4: Variance analysis of the FD and RSD.

Indexes	Factors	SS	df	MS	F	F_α		Significance
						$F_{0.05}$	$F_{0.01}$	
FD	A	345.074	2	172.537	18.824	6.94	18	**
	B	441.277	2	220.639	24.071	6.94	18	**
	C	10.066	2	9.166				
	e	26.599	2					
	e^Δ	36.665	4					
RSD	A	0.427	2	0.214	26.750	19	99	**
	B	0.320	2	0.160	20.000	19	99	**
	C	0.024	2	0.012	1.500	19	99	*
	e	0.016	2	0.008				

Note: e^Δ represents the sum of errors; A: moving speed; B: rotating torque; C: preload.

In other words, for the two test indexes, the smaller improves the effect of the STB sensing of the terrain profile better. The order of importance of the influence FD was $B_1 > A_3 > C_1$, and the order of importance of the influence RSD was $A_3 > B_3 > C_1$. The results of the variance analysis were consistent with those of the range analysis.

4.3. Regression Analysis Prediction Mode. Regression analysis is a predictive modeling technology that analyzes research test indexes and related factors to determine their empirical equations, predict the causal relationship between dependent and independent variables, and provide mathematical prediction models for applications. According to the research in the previous section, it was found that the test indices and test factors were not linear. Therefore, we adopted a nonlinear regression model. In order to simplify the regression analysis model, we eliminate the secondary influencing factors, and focus on the influencing factors of moving speed (A) and rotating torque (B), which are used as independent variables, and their interaction is considered for multivariate nonlinear regression fitting,

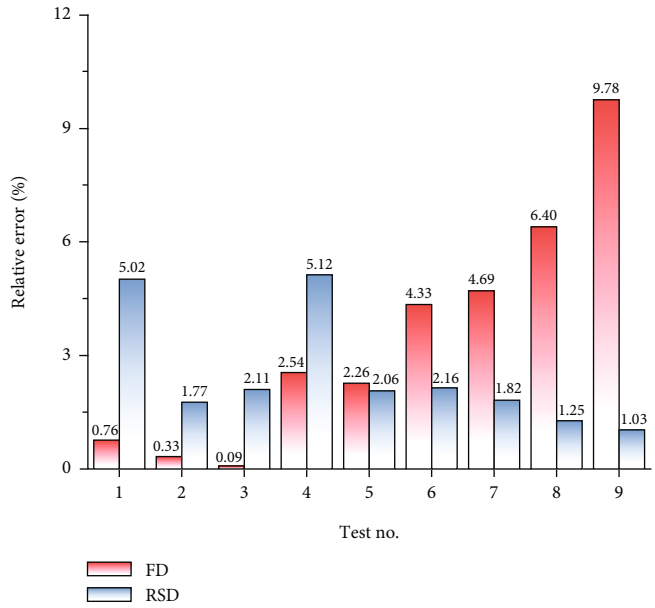

Figure 9: Relative error analysis of test data and prediction data.

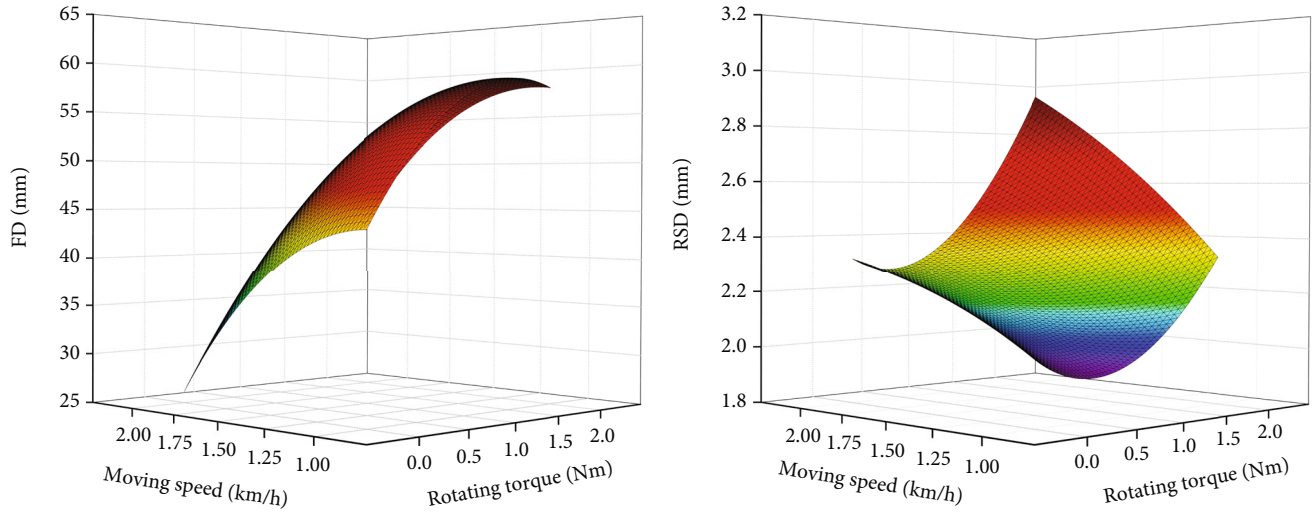

(a) FD (b) RSD

Figure 10: Surface plot of regression prediction model.

and its quadratic model expression is [33]

$$y = \beta_0 + \beta_1 A + \beta_2 B + \beta_{11} A^2 + \beta_{12} AB + \beta_{22} B^2 + \varepsilon, \quad (7)$$

where y is the test index; A and B are the test factors, respectively; $\beta_0, \beta_1, \beta_2, \beta_{11}, \beta_{12}$, and β_{22} are the unknown regression coefficients, and ε is the random error. According to the combination of test factors and indexes results in Table 2, the regression model equation obtained is

$$\begin{cases} \text{FD} = 26.81338 + 33.70059A + 16.52415\text{B} - 17.0225A^2 - 5.57879B^2 + 1.70095AB, \\ \text{RSD} = 5.18767 - 3.19631A - 0.23855B + 0.88183A^2 - 0.04224B^2 + 0.05283AB, \end{cases} \quad (8)$$

The fitting regression equation coefficient of FD was $R^2 = 0.999$, and the fitting regression equation coefficient of RSD was $R^2 = 0.992$. It can be observed that the fitting degree of the two regression equations is very high. To further test the reliability of the regression equation, the horizontal values in Table 2 are introduced into Equation (8), and the relative error of the calculated predicted value and the actual test measurement value are compared to verify the validity of the regression model, as shown in Figure 9. As shown in Figure 9, the largest relative errors in the prediction model errors of the nine groups of FD and RSD were 9.78% and 5.12%, respectively; the smallest relative errors were 0.09% and 1.03%; and the average relative errors were 3.46% and 2.48%, respectively.

The surface diagram of the two indexes is drawn according to Equation (8), as shown in Figure 10. It can be observed

intuitively that the improvement in moving speed has a positive impact on FD and RSD. However, with an increase in the rotating torque, FD continues to increase, resulting in a decrease in the curve similarity. This phenomenon can be verified from the range analysis in Section 4.1 and the variance analysis in Section 4.2. For the actual situation of the field application of a sugarcane harvester, it is necessary to comprehensively analyze the two indexes through the prediction model of regression analysis to obtain the best operation parameters for the matching design. In order to ensure that FD and RSD are relatively minimum when the moving speed and rotating torque are at the same value, a MATLAB optimal model is usually used for optimization, and the optimal value ranges of moving speed (km/h) and rotating torque (Nm) are (1.57, 1.75) and (0.73, 0.86), respectively.

4.4. Discussion. In the orthogonal test results in Section 3, the challenges of the STB in the test and the problems to be solved in the later control system of the sugarcane harvester are clearly demonstrated. In Figure 7, the red curve (ID) and blue curve (STB) overlap is the ideal effect. However, in the nine experiments, the blue curve has obvious response lag and height difference, which leads to an increase in the FD. In addition to the high dependence on the sampling sample, it is likely that this problem is caused by the bottom arc radius r ignored in Section 2.1. This is because the test device only moves horizontally on the track and cannot realize vertical adjustment. However, in practical applications, the terrain sensing device is installed on the base cutter mechanism, and the initial angle θ of the STB is the fixed cutting height; moreover, it is always maintained as the control object. As the terrain fluctuates, if the initial angle θ of the STB changes, the hydraulic cylinder will expand and contract immediately to adjust the height of the base-cutter and restore the angle θ to realize the process of the base cutter height control. Therefore, there will be no change in the contact point between the STB and the soil with the rotation. To eliminate or reduce the influence of bad contact errors, optimization can be considered in the structure of the towed board in a later stage, such as reducing the radian of the bottom.

According to the analysis of introduction, it is clear that the non-contact perception mode is not ideal for dealing with disturbances. In the future, if there are non-contact methods with application value to sugarcane harvesting, such as image recognition technology with complex background features or electromagnetic wave technology penetrating interferents [34], it can be our next research goal. However, at this stage, unless the sugarcane harvesting process is reformed, although the uncertainty in the practical application of contact methods is much more difficult than that of non-contact methods, according to our experimental analysis, Suomi et al. also confirmed that the contact measurement method is a more suitable solution for the analysis of the tillage depth test of the planter [16].

Therefore, for the special agricultural machinery and harvesting technology of sugarcane harvester, it can avoid the adverse effects of interferents relatively better, and our method offers enhanced research value, economy, and applicability. However, it may not offer better advantages in the harvesting method of other crops or a large-scale flat farmland. Secondly, the installation position of the terrain sensing device and treatment method of sugarcane harvester when reversing frequently are also worth discussing in applications. In addition, the influencing factors such as soil moisture and compactness may also affect the sensing effect, and this requires further research. Moreover, the test method proposed in this study is also applicable to the impact analysis of these factors. In addition to the objective factors, the mechanical structural wear of the terrain sensing device and the looseness and offset of the sensor also require regular maintenance and calibration.

5. Conclusions

In this study, a simple and applicable contact terrain sensing device was designed. Through the dynamic analysis of the STB, the influencing factors of the experiment were determined, and the $L_9(3^4)$ orthogonal test scheme was designed with three factors and three levels: the index system of curve similarity (FD) and curve fitting (RSD). The influence of test factor parameters on the terrain perception effect was studied to verify the feasibility of the device relying on the sugarcane harvester to perceive sugarcane field terrain. Finally, according to the orthogonal test results, the degree of influence of the test factors on the test indexes was analyzed via range analysis, variance analysis, and regression analysis. The following conclusions were drawn from the research results:

(i) The rotating torque (factor B) has the greatest influence on the FD of the curve; the moving speed (factor A) has little influence, and the preload (factor C) has the least influence. The moving speed (factor A) and rotating torque (factor B) have significant effects on the RSD of the curve, while the preload (factor C) has little effect

(ii) Both FD and RSD decrease with an increasing moving speed (factor A). However, this does not mean that the faster the moving speed, the better the effect. On the one hand, it is due to the harvest process limitations of the sugarcane harvester. On the other hand, it will reduce the sampling points and lead to terrain perception distortion. Furthermore, although an increase in rotating torque (factor B) leads to an increase in FD, but it helps to reduce the RSD and improve the robustness of the terrain sensing device

(iii) Through regression analysis, a prediction regression model of FD and RSD was obtained with a significant effect and a high fitting degree. Simultaneously, the quantitative relationship between FD and RSD and the two parameters of moving speed and rotating torque could be accurately characterized

(iv) In the practical application of sugarcane harvesters, considering the influence of test factors on the test indexes, the relative minimum values of the two

indexes were taken, and after data processing, the value intervals of the moving speed and the rotating torque are (1.57, 1.75) and (0.73, 0.86), respectively, The terrain perception device can obtain a relatively ideal perception effect

Data Availability

The data used to support the findings of this study are included within the article.

Conflicts of Interest

The authors declare that there is no conflict of interest regarding the publication of this paper.

Acknowledgments

This research was funded by the Scientific and Technological Project of the Department of Transport of Guangxi Province (19-09), the Shaanxi Province Natural Science Foundation (No. 2020JM-249), the Shaanxi Transportation Science and Technology Directorate Plan Project (No. 20-30k), and the Shaanxi Provincial Innovation Capacity Support Plan (No. 2022PT-30). The authors would like to acknowledge Trans-Power Hydraulic Engineering Xi'an Co., Ltd. (China) and Guangxi Fuyu Intelligent Agricultural Machinery Co. Limited, who provided the sugarcane harvester, testing platform, and farm for the research.

References

[1] C. Giachini, C. Ramos, G. Lyra, C. Gamero, and K. Lanças, "Fuel consumption and loss of sugar cane during daytime and nighttime harvesting," *Energia Na Agricultura*, vol. 31, p. 10, 2015.

[2] R. Noronha, R. Silva, C. Chioderoli, E. Santos, and M. Cassia, "Controle estatístico aplicado ao processo de colheita mecanizada diurna e noturna de cana-de-açúcar," *Bragantia*, vol. 70, no. 4, pp. 931–938, 2011.

[3] S. Ma, M. Karkee, P. Scharf, and Q. Zhang, "Sugarcane harvester technology: a critical overview," *Applied Engineering in Agriculture*, vol. 30, no. 5, pp. 727–739, 2014.

[4] D. He, Q. Liu, L. Li, and J. Miao, "Research on intelligent cane-end cutting based on image processing for sugarcane," *Advanced Materials Research*, vol. 320, pp. 631–635, 2011.

[5] Y. Ji, S. Li, C. Peng, H. Xu, R. Cao, and M. Zhang, "Obstacle detection and recognition in farmland based on fusion point cloud data," *Computers and Electronics in Agriculture*, vol. 189, p. 106409, 2021.

[6] L. F. Maldaner, J. P. Molin, T. F. Canata, and M. Martello, "A system for plant detection using sensor fusion approach based on machine learning model," *Computers and Electronics in Agriculture*, vol. 189, no. 4, p. 106382, 2021.

[7] Y. K. Chang, Q. Zaman, A. Farooque, T. Rehman, and T. Esau, "An on-the-go ultrasonic plant height measurement system (UPHMS II) in the wild blueberry cropping system," in *2016 ASABE Annual International Meeting*, p. 1, ASABE, St. Joseph, MI, 2016.

[8] S. Nielsen, L. Munkholm, M. Lamandé, M. Nørremark, G. Edwards, and O. Green, "Seed drill depth control system for precision seeding," *Computers and Electronics in Agriculture*, vol. 144, pp. 174–180, 2018.

[9] H. Liu, A. Reibman, A. Ault, and J. Krogmeier, "Video-based prediction for header-height control of a combine harvester," in *2019 IEEE Conference on Multimedia Information Processing and Retrieval (MIPR)*, pp. 310–315, San Jose, CA, USA, 2019.

[10] J. Li, Y. Zhuang, Q. Peng, and L. Zhao, "Pose estimation of non-cooperative space targets based on cross-source point cloud fusion," *Remote Sensing*, vol. 13, no. 21, p. 4239, 2021.

[11] T. Podmore and L. Huggins, "An automated profile meter for surface roughness measurements," *Transactions of ASAE*, vol. 24, no. 3, pp. 663–665, 1981.

[12] A. Saleh, "Soil roughness measurement: chain method," *Journal of Soil and Water Conservation*, vol. 48, no. 6, pp. 527–529, 1993.

[13] S. Merrill, "Comments on the chain method for measuring soil surface roughness: use of the chain set," *Soil Science Society of America Journal (SSSAJ)*, vol. 62, no. 4, pp. 1147–1149, 1998.

[14] L. Thomsen, J. Baartman, R. Barneveld, T. Starkloff, and J. Stolte, "Soil surface roughness: comparing old and new measuring methods and application in a soil erosion model," *SOIL Discussions*, vol. 1, no. 1, pp. 399–410, 2015.

[15] Y. Xie, A. G. Alleyne, A. Greer, and D. Deneault, "Fundamental limits in combine harvester header height control," *Journal of Dynamic Systems, Measurement, and Control*, vol. 135, no. 3, pp. 345031–345038, 2013.

[16] P. Suomi and T. Oksanen, "Automatic working depth control for seed drill using ISO 11783 remote control messages," *Computers and Electronics in Agriculture*, vol. 116, pp. 30–35, 2015.

[17] B. Xie, H. Li, Z. Zhu, and E. Mao, "Measuring tillage depth for tractor implement automatic using inclinometer," *Transactions of the Chinese Society of Agricultural Engineering*, vol. 29, no. 4, pp. 15–21, 2013.

[18] J. Xia, D. Li, G. Liu, J. Cheng, K. Zheng, and C. Luo, "Design and test of electro-hydraulic monitoring device for hitch tillage depth based on measurement of tractor pitch angle," *Transactions of the Chinese Society for Agricultural Machinery*, vol. 52, no. 8, pp. 386–395, 2021.

[19] L. Zhang, L. Zou, D. Wen, X. Wang, F. Kong, and Z. Piao, "Investigation of the effect of process parameters on bone grinding performance based on on-line measurement of temperature and force sensors," *Sensors*, vol. 20, no. 11, p. 3325, 2020.

[20] S. Yao, J. Deng, D. Sheng, X. Jia, and S. Lu, "Optimization design and analysis of heat pipe internal factors based on the orthogonal test method," *Advanced Materials Research*, vol. 960-961, pp. 349–352, 2014.

[21] R. P. Viator, E. P. Richard, B. J. Viator, W. Jackson, H. L. Waguespack, and H. S. Birkett, "Sugarcane chopper harvester extractor fan and ground speed effects on yield and quality," *Applied Engineering in Agriculture*, vol. 23, no. 1, pp. 31–34, 2007.

[22] M. Martins, J. Testa, F. Drudi, J. Sandi, C. Ramos, and K. Lanças, "Interference of speed at cutting height and damage to rootstock in mechanical harvesting of sugarcane," *Australian Journal of Crop Science*, vol. 13, pp. 1305–1308, 2019.

[23] M. B. Martins, A. C. M. Filho, F. S. Drudi, F. P. . A. P. Bortolheiro, E. P. Vendruscolo, and M. S. T. Esperancini, "Economic efficiency of mechanized harvesting of sugarcane at different operating speeds," *Sugar Tech*, vol. 23, no. 2, pp. 428–432, 2021.

[24] O. Yinggang, M. Wegener, Y. Dantong et al., "Mechanization technology: the key to sugarcane production in China," *International Journal of Agricultural and Biological Engineering*, vol. 6, no. 1, 2013.

[25] Y. Chen, D. Qin, X. Wang, H. Liang, and Y. Feng, "The tracking control for walking speed of sugarcane combine harvester by cutting speed," *Chinese Hydraulics & Pneumatics*, vol. 4, pp. 9–14, 2020.

[26] C. Zhou, "Detecting suspected epidemic cases using trajectory big data," *CSIAM Transactions on Applied Mathematics*, vol. 1, no. 1, pp. 186–206, 2020.

[27] A. Bombelli, L. Soler, E. Trumbauer, and K. Mease, "Strategic air traffic planning with Fréchet distance aggregation and rerouting," *Journal of Guidance, Control, and Dynamics*, vol. 40, no. 5, pp. 1117–1129, 2017.

[28] A. Ismail, S. Abdlerazek, and I. M. El-Henawy, "Development of smart healthcare system based on speech recognition using support vector machine and dynamic time warping," *Sustainability*, vol. 12, no. 6, pp. 2403–2418, 2020.

[29] H. Alt and M. Godau, "Computing the Fréchet distance between two polygonal curves," *International Journal of Computational Geometry & Applications*, vol. 5, no. 1n2, pp. 75–91, 1995.

[30] T. Eiter and H. Mannila, *Computing discrete Frechet distance*, Tecnical University of Vienna, 1994.

[31] H. Weng, S. Wang, Y. Wan, X. Lin, Z. Li, and J. Huang, "Discrete Frechet distance algorithm based criterion of transformer differential protection with the immunity to saturation of current transformer," *International Journal of Electrical Power & Energy Systems*, vol. 115, p. 105449, 2020.

[32] C. Howard, C. Wallace, J. Abbas, and D. Stokic, "Residual standard deviation: validation of a new measure of dual-task cost in below-knee prosthesis users," *Gait & Posture*, vol. 51, pp. 91–96, 2017.

[33] K. Y. Liang and S. L. Zeger, "Regression analysis for correlated data," *Annual Review of Public Health*, vol. 14, no. 1, pp. 43–68, 1993.

[34] L. Zhao, J. Zhang, S. Jiao, T. Zheng, J. Li, and T. Zhao, "Ground surface detection method using ground penetrating radar signal for sugarcane harvester base-cutter control," *Biosystems Engineering*, vol. 219, pp. 103–123, 2022.